

# A CORRECTIVE FRAMEWORK FOR FACIAL FEATURE DETECTION AND TRACKING

Hussein O. Hamshari, Steven S. Beauchemin

*Department of Computer Science, University of Western Ontario, 1151 Richmond Street, London, Canada  
hohamsha@uwo.ca, beau@csd.uwo.ca*

Denis Laurendeau

*Department of Electrical and Computer Engineering, Université Laval, Québec, Canada  
laurend@gel.ulaval.ca*

Normand Teasdale

*Departement de Medecine Sociale et Preventive Faculte de Medecine, Université Laval, Québec, Canada  
normand.teasdale@kin.msp.ulaval.ca*

**Keywords:** Face, facial feature, recognition, detection, tracking, corrective tracking, integrated framework, real-time.

**Abstract:** Epidemiological studies indicate that automobile drivers from varying demographics are confronted by difficult driving contexts such as negotiating intersections, yielding, merging and overtaking. We aim to detect and track the face and eyes of the driver during several driving scenarios, allowing for further processing of a driver's visual search pattern behavior. Traditionally, detection and tracking of objects in visual media has been performed using specific techniques. These techniques vary in terms of their robustness and computational cost. This research proposes a framework that is built upon a foundation synonymous to boosting. The idea of an integrated framework employing multiple trackers is advantageous in forming a globally strong tracking methodology. In order to model the effectiveness of trackers, a confidence parameter is introduced to help minimize the errors produced by incorrect matches and allow more effective trackers with a higher confidence value to correct the perceived position of the target.

## 1 INTRODUCTION

Our study of visual patterns of interest in drivers is facilitated through the development of a robust computer vision system. The intelligent system, developed as part of this project, is aimed at reinforcing behaviors characterizing skilled drivers separate from behaviors that are sub-optimal. To achieve such an objective, new methods and tools are developed based on the extraction of three types of information from video streams captured during driving scenarios: head motion in 3D space, eye motion (gazing), and facial expressions of the driver in response to different stimuli.

The camera setup for this project allows for several computer vision applications. Figure 1 shows the schematics for the simulator and how the cameras are put together to provide maximum knowledge of the surrounding environment. The computer vision system is comprised of: *i)* A set of three Black & White firewire video cameras, *ii)* an infrared lighting system,

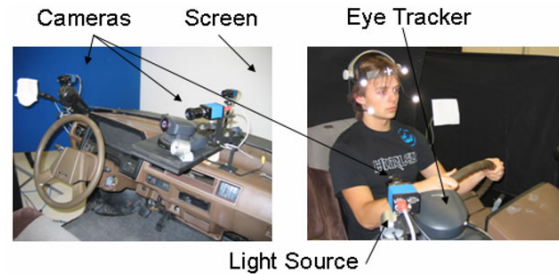


Figure 1: The simulator setup showing the different components used for data acquisition.

*iii)* a virtual reality screen onto which the driving scenarios are projected (Figure 2), and *iv)* an eye tracker camera.

Given the various tasks set out for the project, this contribution is only concerned with the detection and tracking of selected facial features in the given video sequences from the three camera inputs. We aim to



Figure 2: Virtual reality screens showing different driving contexts: **left**) Pedestrians crossing the street, and **right**) a bus stopped on the roadside.

detect and track the face and eyes of the driver during several driving scenarios, allowing for further processing of a driver’s visual search pattern behavior. Figure 3 shows the input from the three cameras.

## 2 BACKGROUND

The techniques developed by Leinhardt and Maydt (Leinhardt and Maydt, 2002) extend upon a machine-learning approach that has originally been proposed by Viola and Jones (Viola and Jones, 2001). The rapid object detector they propose consists of a cascade of boosted classifiers. Boosting is a machine learning meta-algorithm used for performing supervised learning. These boosted classifiers are trained on simple Haar-like, rectangular features chosen by a learning algorithm based on AdaBoost (Freund and Schapire, 1995). Viola and Jones have successfully applied their object detection method to faces (Viola and Jones, 2004), while Cristinacce and Cootes (Cristinacce and Cootes, 2003) have used the same method to detect facial features. Leinhardt and Maydt extend the work of Viola and Jones by establishing a new set of rotated Haar-like features which can also be calculated very rapidly while reducing the false alarm rate of the detector. In the techniques proposed by Zhu and Ji (Zhu and Ji, 2006), a trained AdaBoost face detector is employed to locate a face in a given scene. A trained AdaBoost eye detector is applied onto the resulting face region to find the eyes; a face mesh, representing the landmark points model, is resized and imposed onto the face region as a rough estimate. Refinement of the model by Zhu and Ji is accomplished by fast phase-based displacement estimation on the Gabor coefficient vectors associated with each facial feature. To cope with varying pose scenarios, Wang et al. (Wang et al., 2006) use asymmetric rectangular features, extended by Wang et al. from the original symmetric rectangular features described by Viola and Jones to represent asymmetric gray-level features in profile facial images.

Shape modeling methods for the purpose of facial feature extraction are common among computer vision systems due to their robustness (Medioni and Kang, 2005). Active Shape Models (Cootes et al., 1995) (ASM) and Active Appearance Models (Cootes et al., 1998) (AAM) possess a high capacity for facial feature registration and extraction. Such efficiency is attributed to the flexibility of these methods, thus compensating for variations in the appearance of faces from one subject to another (Ghrabieh et al., 1998). However, a problem displayed by both ASM and AAM techniques is the need for initial registration of the shape model close to the fitted solution. Both methods are prone to local minima otherwise (Cristinacce and Cootes, 2004). Cristinacce and Cootes (Cristinacce and Cootes, 2006) use an appearance model similar to that used in AAM, but rather than approximating pixel intensities directly, the model is used to generate feature templates via the proposed Constrained Local Model (CLM) approach. Kanaujia et al. (Kanaujia et al., 2006) employ a shape model based on Non-negative Matrix Factorization (NMF), as opposed to Principal Component Analysis (PCA) traditionally used in ASM methods. NMF models larger variations of facial expressions and improves the alignment of the model onto corresponding facial features. Since large head rotations make PCA and NMF difficult to use, Kanaujia et al. use multi-class discriminative classifiers to detect head pose from local face descriptors that are based on Scale Invariant Feature Transforms (SIFT) (Lowe, 1999). SIFT is typically used for facial feature point extraction on a given face image and works by processing a given image and extracting features that are invariant to the common problems associated with object recognition such as scaling, rotation, translation, illumination, and affine transformations.

## 3 TECHNIQUE DESCRIPTION

Our approach makes use of several techniques for processing input sequences of drivers following given scenarios in the simulator. Such techniques have been used successfully on their own (Leinhardt and Maydt, 2002; Lowe, 1999) and as part of a more extended framework (Kanaujia et al., 2006). Acceptable face and facial feature detections were produced at good success rates. Each technique used in our framework is treated as a module and these modules are classified into two major groups: detectors, and trackers. Detectors localize the facial regions automatically and lay a **base image** to be used for tracking by other modules. A base image is a visual capture of a particular facial



Figure 3: Visual input taken from the three cameras mounted on the simulator.

region and can be used to perform a match against several other regions throughout the input sequence. Trackers use the base image set out by the detectors and employ matching algorithms to retrieve the correct position of the same facial region across following frames. Our framework uses a tracker based on Scale-Invariant Feature Transform (SIFT) (Lowe, 1999) and a second tracker that uses a normalized correlation coefficient (NCC) method as follows:

$$\tilde{R}(x, y) = \frac{\sum_{y'=0}^{h-1} \sum_{x'=0}^{w-1} \tilde{T}(x', y') \tilde{I}(x+x', y+y')}{\sqrt{\sum_{y'=0}^{h-1} \sum_{x'=0}^{w-1} \tilde{T}(x', y')^2 \sum_{y'=0}^{h-1} \sum_{x'=0}^{w-1} \tilde{I}(x+x', y+y')^2}}$$

where  $\tilde{T}(x', y') = T(x', y') - \bar{T}$ ,  $\tilde{I}(x+x', y+y') = I(x+x', y+y') - \bar{I}$ , and where  $\bar{T}$  and  $\bar{I}$  stand for the average value of pixels in the template raster and current window of the image, respectively.  $T(x, y)$  is the value of the template pixel in the location  $(x, y)$  and  $I(x, y)$  is the value of the image pixel in the location  $(x, y)$ .

The rapid object detector (ROD) proposed by Viola and Jones (Viola and Jones, 2001) is a hybrid in that it can be classified as both a detector and tracker; it is employed to detect the face and localize the eyes, while the SIFT and NCC trackers only deal with the eye regions. Often, a tracker in our framework may lose a target due to fast movement of the driver's head; a false positive base image may be registered at that time and the **off-target** tracker may eventually be tracking the wrong region as a consequence. As a detector, the ROD localizes the face and facial features automatically. As a tracker, it is used to track the eyes in between frames and to correct off-target trackers allowing for a second registration of a base image. Figure 4 shows an example of how a tracker can lose its target and provide misleading information with regards to the position of the eyes. One could argue that only one registration of the base image should be used. However, given that the classifier is not perfect, and is vulnerable according to its associated false positive rate, the base image registered could be an invalid region of the face, incorrectly per-

ceived as an eye. Several base image registrations are therefore needed along the sequence.

The framework uses a look-up table composed of blurred, scaled down Gaussian images. The Gaussian pyramid method (Burt and Adelson, 1983) creates a stack of images that are successively smaller; the base image of the pyramid is defined as the original image and each image at any given level is composed of local averages of pixel neighborhoods of the preceding level of the pyramid. Detectors employed in our framework process the highest level of the pyramid first. In the case where an object of interest is not detected, the next level down is processed in a similar manner. The bottom-up approach used to detect faces and eyes in our framework reduces the processing time required by the detectors.

The three cameras available on the cockpit of the simulator provide all views of the driver necessary to achieve continuous tracking: A tracker may lose its target if the driver was to check his/her blind spot, but given the camera setup installed onto the cockpit, a driver can be studied at all times. In order to achieve continuous tracking, the framework must detect a change in a driver's head pose, and act upon such an event accordingly by flipping between the available views. For each frame that is processed by the ROD tracker, the framework keeps track of the number of hits and misses for the left  $m_L$  and right  $m_R$  eyes within a detected face. Hits lower the value of  $m_L$  or  $m_R$  whereas misses increase their values accordingly. A switch from one view to another occurs when the value of either  $m_L$  or  $m_R$  exceeds a certain threshold  $\tau$ , signifying that one (or two) of the eyes are being missed, leading to the conclusion that a head pose is in progress. Depending on which eye has been repeatedly missed, the appropriate view is placed as the primary view and processed until another switch is needed.

### 3.1 Corrective Tracking

The various methods used in our framework produce good results, whether for detecting or tracking objects



Figure 4: An example sequence where a tracker loses its target, performed on an annotated sequence of a talking face, available at Dr. Tim Cootes’ website (Cootes, 2007). From left to right: **a)** The eyes, the tracker’s target in this case, have been acquired and are tracked throughout several frames, **b)** the person’s head moved by a significant amount and a base image was registered according to the interval set, **c)** and, since the base image, registered by the tracker, is a false positive, tracking is now being performed on the wrong region of the face.

of interest in a given scene. The quality of the Haar-based classifier used by the rapid object detector is determined by its ability to correctly predict classifications for unseen (negative) examples. The classifier must be evaluated with a set of examples that is separate from the training set of samples used to build it. In many cases, some of the negative examples that should be used during the training phase of the classifier are missed and, in such a case, errors are introduced when the same negative example is seen by the classifier. Detectors and trackers can be corrective in that errors introduced by one module in our framework are likely to be corrected by one or more of the modules throughout the input sequence. An off-target tracker can be corrected by a hybrid detector/tracker in order to allow for a second registration of a base image of the eye and, vice versa, where a false positive detection of the eye region by the hybrid detector/tracker can be rectified by one or more trackers with a true positive base image.

The framework has been designed with growth in mind: extra trackers may need to be added to increase the accuracy of the system as a whole. A fourth tracker has been developed to illustrate the ease of adding extra components to the framework. The fourth tracker simply searches for the lowest average intensity over a  $m \times n$  neighborhood of pixels in a given region of interest; this operation, given a region close to the eyes, translates to finding the darkest areas in that region. Hence, the tracker now acts as a naive Pupil Finder (PPL). A possible problem could occur when the PPL tracker targets the eyebrows rather than the pupil when considering the darkest regions; both the pupils and the brows display comparable neighborhood intensities and can be mistaken for one another by the naive tracker. However, given that there are other correcting trackers employed by the framework, such problems can be easily and automatically

rectified by the other trackers. It is important to note that the PPL method is less vulnerable to the off-target tracking problem discussed previously mainly due to the fact that it does not use a base image to perform the search. Thus, an off-target PPL can be set on-target by any given detector through a single true positive detection.

### 3.2 Confidence Parameter

Trackers process each eye separately. Once a tracker processes a given frame within the input sequence, a displacement vector  $\vec{v}$  is produced, which tells the distance from the previous position of the eye to its new position at the most recent frame, and the detection window is placed accordingly. Since the accuracy of each tracker differs, a **confidence parameter**  $\omega$  is introduced to restrict weak trackers from incorrectly displacing the detection window. The SIFT tracker, for example, is more reliable than the NCC tracker and, as a result, should be given a higher confidence value than that of NCC.

Given the trackers used by our framework, three displacement vectors are produced: The ROD tracker vector  $\vec{v}_R$ , the SIFT tracker vector  $\vec{v}_S$ , the NCC tracker vector  $\vec{v}_N$ , and the PPL tracker vector  $\vec{v}_P$ . Additionally, three associated confidence parameters are set for each of the trackers:  $\omega_R$ ,  $\omega_S$ ,  $\omega_N$ , and  $\omega_P$ . Applying a separate confidence parameter to each of the vectors produced by the trackers minimizes the errors produced by incorrect matches and allows trackers with a higher confidence value to correct the perceived position of the eye through the displacement of the detection window. The displacement of the detection window is then computed as follows:

$$\vec{V}_t = \frac{\sum_{i=0}^n \omega_i \vec{v}_i}{\sum_{i=0}^n \omega_i} \quad (1)$$

where  $n$  is the total number of trackers employed,  $\omega_i$  and  $\vec{v}_i$  are the associated confidence parameter and displacement vector, respectively, for tracker  $i$ , and  $\vec{V}_t$  is the final displacement vector produced after processing frame  $t$ . (1) assumes that each tracker  $i$  produces a displacement vector  $\vec{v}_i$  based on the processing of the same exact region  $R(x,y)$  of the eyes at each frame. The computational cost of running all the trackers at each frame is great; Section 3.3 illustrates how (1) can be simplified to increase the performance of the framework.

### 3.3 Interval Parameter

Running all trackers in our framework at every frame is computationally expensive. A more efficient solution is to only employ a single tracker at any given frame, as it helps increase the frame rate and produce smoother movement of the detection window. An **interval parameter**  $\kappa$  is given to each tracker. The NCC tracker can be run at more frequent intervals in the framework than SIFT and, as a result, can be given a smaller interval parameter. In addition to the confidence parameter, the definition of long-term, short-term, and real-time corrective tracking are extended to include the interval parameter.

Given the three trackers used by our framework, three interval parameters are assigned:  $\kappa_R$ ,  $\kappa_S$ ,  $\kappa_N$ , and  $\kappa_P$ . Since some of the components of our framework, namely the SIFT and NCC trackers, need to register a base image to employ their matching algorithms on their assigned frames, two additional interval parameters are set:  $\kappa_{S_{base}}$  and  $\kappa_{N_{base}}$ . The overall timeline is reflected in Figure 5.

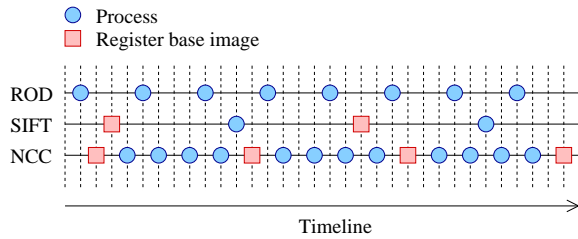


Figure 5: An example of a processed timeline according to the assigned interval parameters for each of the three tracking component in our framework.

Since each frame in the sequence is only processed by one component in our framework, dictated by the interval parameters given to each tracker, (1) is simplified as follows:

$$\vec{V}_t = \omega_i \vec{v}_i \quad (2)$$

Addition of the vectors is eliminated from the

computation of (1) since each frame  $t$  is only processed by a single tracker  $i$ .

### 3.4 Integration Algorithm

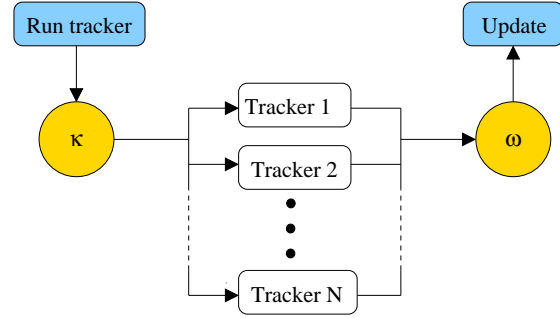


Figure 6: An overview of the tracker selection process employed by our framework.

The following describes, in detail, the algorithm employed by our framework:

1. **Acquire new frame:** Given the selected view thought to contain a face, a new frame is acquired.
2. **Build Gaussian pyramid:** Once a new frame is acquired, a Gaussian pyramid is built according to Section 3.
3. **Detect a face:** The face detector is applied to the entire scene, in search of a profile face.
4. **Track the eyes:** If the eyes have not been detected by the system yet, the eye detector is run on the regions of interest. In the case where the eyes have already been registered by the trackers, the system employs the appropriate tracker on the ROI, according to the associated interval  $\kappa$ .
5. **Update detection windows:** The detection window for the left and right eyes are updated according to the displacement vector produced by the tracker employed, and adjusted using the confidence parameter  $\omega$  associated with the tracker. Figure 6 illustrates the tracker selection process.
6. **View switching assessment:** Once the frame has been fully processed, results from the detectors and some of the trackers are used to assess the current, primary view, according to the thresholds set in Section 3. A view switch is performed if necessary.

## 4 RESULTS

To accurately determine the true positive and false positive rates, our framework needs to compute the



number of true and false positives as well as the number of true and false negatives; this is shown in Figure 7. The computation of true (or false) positives (or negatives) is performed at a fine pixel level to achieve accuracy. The number of true positives, for example, is calculated as the area where the detected and actual (ground truth) regions intersect, outlined in green on Figure 7. The true positive rate (or sensitivity) is computed as:

$$\alpha_T = \frac{TP}{TP + FN} \quad (3)$$

where  $TP$  and  $FN$  are the total number of true positives and false negatives found, respectively, and  $\alpha_T$  is the true positive rate in the range  $[0 \dots 1]$ . The false positive rate (or  $1 - \text{specificity}$ ) is computed as:

$$\alpha_F = \frac{FP}{FP + TN} \quad (4)$$

where  $FP$  and  $TN$  are the total number of false positives and true negatives found, respectively, and  $\alpha_F$  is the false positive rate in the range  $[0 \dots 1]$ .

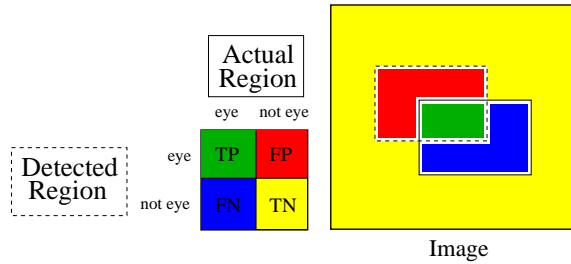


Figure 7: An illustration determining true positives (TP), false positives (FP), true negatives (TN), and false negatives (FN). In the image representation on the right of this figure, the solid-line box shows the true position of a given eye (ground truth), whereas the dashed-line box shows the detected region of the eye.

Computing the true positive and false positive rates at such a fine level provides an accurate representation to be used in plotting the Receiver Operating Characteristic (ROC) curves for our method. However, an actual classification does not need to be described at such a fine pixel level for a true outcome to occur. Figure 8 shows three detection windows. In Figure 8a, the detection window encapsulates the entire region of the eye, and is hence considered to be a hit. Figure 8c is classified as a miss since the detection window deviates almost completely from the eye region, covering only a small fraction of true positives. Figure 8b, however, does cover the majority of the eye region, and therefore can be considered as a hit since it correctly classifies the region as containing an eye.

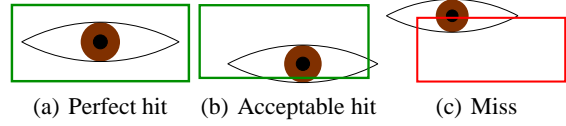


Figure 8: An illustration showing two hits (a) and (b), and one miss (c), in determining whether or not the detection window covers an eye.

As a result, we follow to describe a coarser method for quantifying a hit rate based on whether or not the detection window contains an eye:

$$\alpha_H = \frac{H}{H + M} \quad (5)$$

where  $H$  and  $M$  are the total number of hits and misses, respectively, and  $\alpha_H$  is the hit rate in the range  $[0 \dots 1]$ . The coverage of the number of true positives as a fraction of the actual (ground truth) region of the eye from Figure 7 can be modeled as per (3). To ensure that we also model false positives into our hit-miss classification scheme, the number of true positives as a fraction of the number of false positives is accounted for as follows:

$$\alpha_D = \frac{TP}{FP} \quad (6)$$

where  $TP$  and  $FP$  are the number of true positives and false positives, respectively. The number of hits  $H$  and misses  $M$  can then be computed as follows:

$$S_t = \begin{cases} 1 & (\alpha_{T_t} \geq \rho_T) \wedge (\alpha_{D_t} \geq \rho_D) \\ 0 & \text{otherwise} \end{cases} \quad (7)$$

where  $\alpha_T$  and  $\alpha_D$  are the true positive fractions discussed previously, at frame  $t$ , and  $\rho_T$  and  $\rho_D$  are thresholds by which leniency can be given to how a hit is counted. A hit occurs when  $S$  is 1; otherwise, a miss is counted.

#### 4.1 Confidence Parameter $\omega$

The following experiments were performed to test the performance of the separate methods when using varying values for  $\omega$ ; the values of  $\omega$  were sampled at: 0.1, 0.3, 0.5, 0.7, 0.9, and 1.0. The NCC, SIFT, and PPL methods also employ the ROD method at a less frequent interval to lessen the vulnerability to the off-target tracking problem. The values showing the best, worst, and average levels of performance are shown on Figures 9 to 12. The area under the ROC curve (AUC) was also computed for each curve to outline the accuracy of the methods with respect to the assigned confidence parameters. The AUC values for

the curves in Figures 9 to 12 are summarized in Table 1.

Table 1: The AUC for curves produced when the confidence parameter is varied.

Method	$\omega$	AUC
ROD	0.1	0.878150
	0.7	0.895555
	1.0	0.883620
NCC	0.1	0.883433
	0.3	0.889503
	1.0	0.871861
SIFT	0.1	0.882617
	0.9	0.882617
	1.0	0.891356
PPL	0.1	0.891356
	0.5	0.919164
	1.0	0.930864

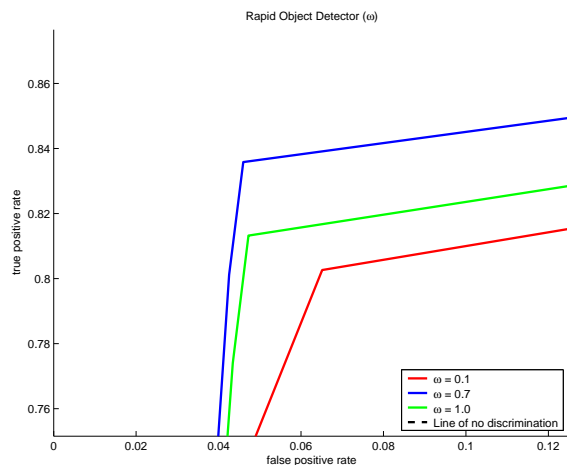


Figure 9: ROC curves for the ROD method showing the three, most descriptive curves.

## 4.2 Framework Integration

The following experiments were done to test the performance of the methods when they are integrated together into a single, corrective framework. The values showing the best, worst, and average levels of performance are shown on Figures 13 and 14. The AUC was also computed for each curve to outline the accuracy of the methods after integration. The AUC values for the curves in Figures 13 and 14 are summarized in Table 2.

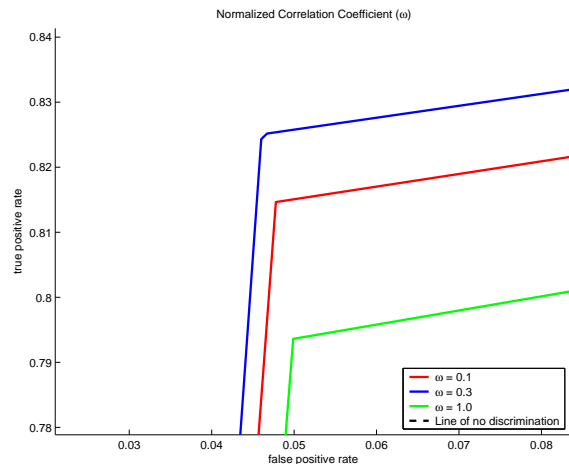


Figure 10: ROC curves for the NCC method showing the three, most descriptive curves.

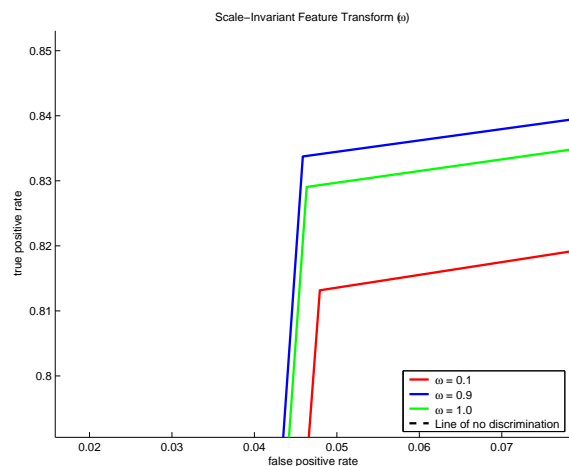


Figure 11: ROC curves for the SIFT method showing the three, most descriptive curves.

## 5 Conclusion

The ROD is run more frequently when it is employed on its own. The NCC, SIFT, and PPL methods employ the ROD method less frequently. As a result, the ROD is meant to produce slightly better results than any of the other methods due to the fact that the detector is run more frequently. Off-target tracking problems help lower the performance of the NCC and SIFT methods, given that the detector is not allowed to run as often as when it is employed on its own (ROD method). The PPL method gives the best results with a 3.5% performance increase over the ROD method. As explained in Section 3.1, the PPL method is less vulnerable to off-target tracking problems, and, as a result, is shown to produce excellent

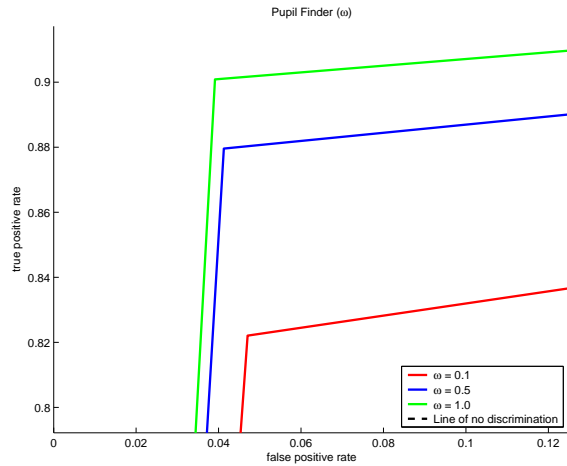


Figure 12: ROC curves for the PPL method showing the three, most descriptive curves.

Table 2: The AUC for curves produced through integration of the various methods.

Method	AUC
ROD	0.879225
ROD + NCC	0.874807
ROD + SIFT	0.877594
ROD + PPL	0.934116
ROD + NCC + SIFT	0.878237
ROD + NCC + SIFT + PPL	0.939404

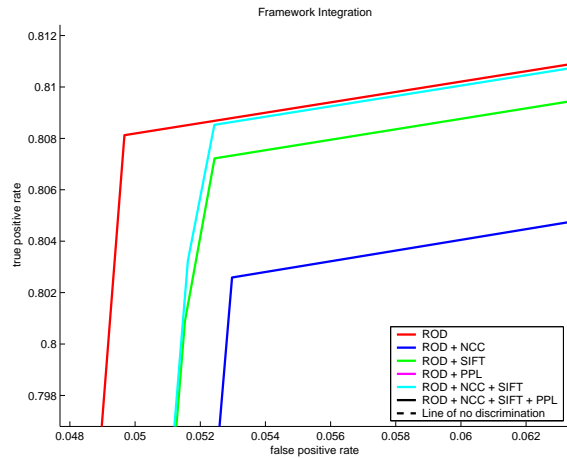


Figure 13: ROC curves showing the performance of the methods employed by the framework, and the integration of those methods into a single, corrective framework. Only ROD, NCC, SIFT, and ROD + NCC + SIFT methods are shown on this graph.

results over the other methods. The SIFT method employs computationally expensive algorithms that

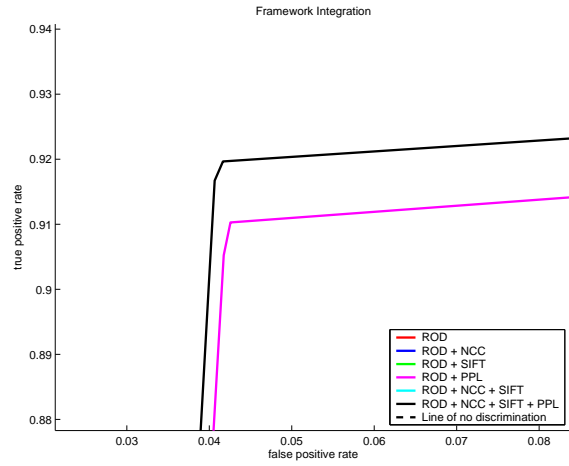


Figure 14: ROC curves showing the performance of the methods employed by the framework, and the integration of those methods into a single, corrective framework. Only PPL and ROD + NCC + SIFT + PPL methods are shown on this graph.

lower the frame rate of the system. As a result, SIFT processes frames at the lowest level of the Gaussian pyramid that is employed in our framework. However, and as can be seen in our results, the performance of the SIFT tracker is also lowered, to maintain an acceptable frame rate.

The confidence parameters were chosen according to the results presented in Section 4.1. The optimal curve with the best AUC value was chosen and the experiments were conducted accordingly. As mentioned previously in this section, the NCC and SIFT methods produced lower results than the ROD method due to the fact that ROD was run more frequently when employed on its own. However, the **integration** of ROD, NCC and SIFT is shown to produce results close to that of the ROD method alone, as can be seen in Figure 13. The PPL method produced the best results when compared to the ROD, NCC, and SIFT methods (all employed individually on top of the ROD method). However, the integration of ROD, NCC, SIFT, and PPL method further increases the performance of the system by 0.5% over the PPL method. The full integration of the methods into a single, corrective framework then shows a performance boost of 6%. In terms of hit rate, which is a measure slightly coarser than the true positive rate (as explained in Section 4), the ROD method, when used alone, produces a hit rate of 92.6285%. However, when integrating the entire set of methods into the framework to work together, the hit rate is increased to 99.4499%.

With a high level of accuracy comes a high level of cost. All the experiments were performed on a lap-



top running a Intel®Pentium®M processor at 2.00 GHz. The mean frame rate when employing the ROD method alone is found to be 16.8835 frames per second. The integration of the methods lowers the frame rate to 12.3193 frames per second. The reason for the low frame rate through integration comes back to the implementation of SIFT, as it is computationally costly. A slight change in configuration of the parameters for the framework could, potentially, produce higher frame rates at excellent performance levels.

This research is based on the hypothesis that visual search patterns of at-risk drivers provide vital information required for assessing driving abilities and improving the skills of such drivers under varying conditions. Combined with the signals measured on the driver's body and on the driving signals of a car simulator, the visual information allows a complete description and study of visual search pattern behavior of drivers.

## REFERENCES

- Burt, P. and Adelson, E. (1983). The laplacian pyramid as a compact image code. In *IEEE Transactions on Communications*, volume 4, pages 532–540.
- Cootes, T. (2007). Images with annotations of a talking face. Available at: [http://www.isbe.man.ac.uk/~bim/data/talking\\_face/talking\\_face.html](http://www.isbe.man.ac.uk/~bim/data/talking_face/talking_face.html). November 4th, 2007.
- Cootes, T., Cooper, D., Taylor, C., and Graham, J. (1995). Active shape models - their training and application. *Computer Vision and Image Understanding*, 61:38–59.
- Cootes, T., Edwards, G., and Taylor, C. (1998). Active appearance models. In *Conf. Computer Vision*, volume 2, pages 484–498.
- Cristinacce, D. and Cootes, T. (2003). Facial feature detection using adaboost with shape constraints. In *Proc. British Machine Vision Conference*, pages 231–240.
- Cristinacce, D. and Cootes, T. (2004). A comparison of shape constrained facial feature detectors. In *Proc. Int. Conf. Automatic Face and Gesture Recognition*, pages 375–380.
- Cristinacce, D. and Cootes, T. (2006). Feature detection and tracking with constrained local models. In *Proc. British Machine Vision Conference*, pages 929–938.
- Freund, Y. and Schapire, R. (1995). A decision-theoretic generalization of on-line learning and an application to boosting. In *European Conference on Computational Learning Theory*, pages 23–37.
- Ghrabieh, R. A., Hamarneh, G., and Gustavsson, T. (1998). Review - active shape models - part ii: Image search and classification. In *Proc. Swedish Symposium on Image Analysis*, pages 129–132.
- Kanaujia, A., Huang, Y., and Metaxas, D. (2006). Emblem detections by tracking facial features. In *Proc. IEEE Computer Vision and Pattern Recognition*, pages 108–108.
- Leinhardt, R. and Maydt, J. (2002). An extended set of haar-like features for rapid object detection. In *Proc. Int. Conf. Image Processing*, volume 1, pages 900–903.
- Lowe, D. (1999). Object recognition from local scale-invariant features. In *Proc. Int. Conf. Computer Vision*, volume 2, page 1150.
- Medioni, G. and Kang, S. (2005). *Emerging Topics in Computer Vision*. Prentice Hall.
- Viola, P. and Jones, M. (2001). Rapid object detection using a boosted cascade of simple features. In *Proc. IEEE Computer Vision and Pattern Recognition*, volume 1, pages 511–518.
- Viola, P. and Jones, M. (2004). Robust real-time face detection. *Int. J. Comput. Vision*, 57:137–154.
- Wang, Y., Liu, Y., Tao, L., and Xu, G. (2006). Real-time multi-view face detection and pose estimation in video stream. In *Conf. Pattern Recognition*, volume 4, pages 354–357.
- Zhu, Z. and Ji, Q. (2006). Robust pose invariant facial feature detection and tracking in real-time. In *Proc. Int. Conf. Pattern Recognition*, volume 1, pages 1092–1095.